Paper:
Di Fraia, S. & Nithiarasu, P. (2019). A generalised model for electro-osmotic flow in porous media. *International Journal of Numerical Methods for Heat & Fluid Flow, ahead-of-print*(ahead-of-print)
http://dx.doi.org/10.1108/HFF-03-2019-0192

International Journal of Numerical Methods for Heat and Fluid Flow

A generalised model for electro-osmotic flow in porous media

Journal:	*International Journal of Numerical Methods for Heat and Fluid Flow*
Manuscript ID	HFF-03-2019-0192.R2
Manuscript Type:	Research Article
Keywords:	Electro-osmosis, Porous media, Charged particles, Generalised model, Fractional step method

A generalised model for electro-osmotic flow in porous media

Abstract

Purpose - This work aims at developing a comprehensive model for the analysis of Electro-Osmotic Flow (EOF) through a fluid saturated porous medium. In order to fully understand and exploit a number of applications, such a model for EOF through porous media is essential.

Design/methodology/approach - The proposed model is based on a generalised set of governing equations used for modelling flow through fluid saturated porous media. These equations are modified to incorporate appropriate modifications to represent electro-osmosis. The model is solved through the Finite Element Method (FEM). The validity of the proposed numerical model is demonstrated by comparing the numerical results of internal potential and velocity distribution with corresponding analytical expressions. The model introduced is also used to carry out a sensitivity analysis of the main parameters that control electro-osmotic flow.

Findings - The analysis carried out confirms that electro-osmosis in free channels without porous obstructions is effective only at small scales, as largely discussed in the available literature. Employing porous media makes electro-osmosis independent of the channel scale. Indeed, as the channel size increases, the presence of the charged porous medium is essential to induce fluid flow. Moreover, results demonstrate that flow is significantly affected by the characteristics of the porous medium, such as particle size, and by the zeta potential acting on the charged surfaces.

Originality/value - To the best of author's knowledge, a comprehensive FEM model, based on the generalised equations to simulate electro-osmotic flow in porous media, is proposed here for the first time.

Paper type - Research paper

Keywords: Electro-osmosis; Porous media; Charged particles; Generalised model; Fractional step method

1 Introduction

Electro-Osmosis (EO) in porous media has been studied for over two centuries, due to its wide range of interests in civil, medical and industrial applications. It is employed for cooling of electronic devices (Berrouche et al., 2009; Cheema et al., 2013), dehumidification, dehydration and regeneration processes of solid desiccant in heating ventilation air conditioning systems (Li et al., 2013a,b), fabrication of micro biomedical technologies (Cheema et al., 2013; Misra and Chandra, 2013), treatments for environmental purposes (Li et al., 2013b; Hlushkou et al., 2005; Shapiro and Probstein, 1993; Wu and Papadopoulos, 2000; Tallarek et al., 2002; Cameselle, 2015), dewatering (Lewis and Garner, 1972; Lewis and Humpheson, 1973), energy production (Cheema et al., 2013; Chen et al., 2014; Bennacer et al., 2007; Mahmud Hasan et al., 2011). In order to understand the physical phenomenon of EO, the concept of Electric Double Layer (EDL) needs to be introduced. A charged surface in contact with an electrolytic solution is usually deprotonated. Since the solid-liquid interface is negatively charged, it attracts the fluid cations that form a high concentration region, called EDL. As the distance from the charged surface increases, the ions concentration decreases and it can be considered equal to that of the bulk solution. The EDL is the main is responsible for EO. When the distance from the charged surface is large compared to the EDL thickness, the velocity is independent of the channel width and constant within the channel. For this reason, EO driven flow systems are mainly related to thin EDLs on charged surfaces. In other words, as the surface to volume ratio increases, Electro-Osmotic Flow (EOF) increases. Therefore, unlike pressure driven flow, where velocity is proportional to the square of the channel width, EO is more effective at micro-scale. In fluid systems, only the channel walls can be considered as electrically active surfaces. When charged solid particles are introduced inside a channel, their surface will also influence the EOF. As a consequence, porous electro-osmotic systems are getting more and more attractive. Indeed in low porosity media, EOF has been found to be effective (Anderson and Keith Idol, 1985) and more advantageous than pressure-driven flows (Hlushkou et al., 2005; Tallarek et al., 2002).

One of the first applications for EOF in porous media has been Capillary ElectroChromatography (CEC), where electro-osmosis is used to drive flow in packed capillary columns (Hlushkou et al., 2005; Tallarek et al., 2002; Rathore and Horváth, 1997; Li and Remcho, 1997; Wan, 1997; Liapis and Grimes, 2000; Hlushkou et al., 2006), instead of hydrostatic pressure as in classical high-performance liquid chromatography systems. While analysing such systems, several parameters are found to influence EOF in porous media. The velocity increases as the applied electrical field increases (Liapis and Grimes, 2000). Also, the wall zeta potential affects the flow, but only within about one third of the capillary radius (Rathore and Horváth, 1997; Liapis and Grimes, 2000). The velocity decreases as the particle diameter increases, with more significant effects noticed at higher differences between the zeta potential of the walls and that of the particles (Liapis and Grimes, 2000). Also, the orientation and contact of fibres in arrays of ordered fibrous porous media (Kozak and Davis, 1986), the concentration and distance of solid particles (Kozak and Davis, 1989; Di Fraia et al., 2017) and the connectivity among the intra-particle pores (Grimes et al., 2000) influence EOF.

Beyond CEC, EO is commonly used for micro-pumping. The analysis in such systems is carried out mainly through analytical models, focused on the maximum pressure, maximum flow rate and efficiency of the pump. The first theory has been introduced by Zeng et al. (2001), and then used as it is or extended by other authors. Yao and Santiago (2003) modified this model, considering two terms composing the total current, the advective and the electromigration currents. The analytical model proposed by Zeng et al. has been used to examine a high-pressure EO micro-pump (Wang et al., 2006) or to compare two types of porous ceramics, sintered alumina and silica, to realize an EO pump (Berrouche et al., 2009). The studies on EO pumps highlight the influence on EOF of pore radius and porosity (Berrouche et al., 2009; Cheema et al., 2013; Yao et al., 2006).

In general, porous medium flow can be studied by using several approximations and assumptions. Depending on the chosen approach, fluid flow in porous media can be investigated at the pore level or by using a macroscopic method. Obviously, the first approach provides minute details of flow, but it is computationally expensive (Massarotti et al., 2003). For this reason, such a method is only employed when the interaction mechanisms at the internal interfaces between the materials that compose the porous medium, need to be accurately determined (Ehlers and Bluhm, 2013). The flow in a homogeneous porous medium can be analysed as a continuum through an appropriate averaging process (Ehlers and Bluhm, 2013), which can be:

- statistical, if the porous medium is averaged over reference porous structures, by assuming a statistical homogeneity;

- spatial, by averaging the medium over the so-called Representative Elementary Volume (REV) (Whitaker, 1967), whose scale, l, is larger than the scale of the porous medium particle, d_p, and smaller than that of the flow domain, L (Nield and Bejan, 2006), as shown in Figure 1.

The basic law governing fluid flow through porous media is Darcy's equation, which linearly relates the pressure gradient to the flow rate across the porous medium (Darcy, 1856). To overcome the limitations of the Darcy theory, several *non-Darcy models* have been introduced. The most common are:

- Forchheimer's equation (Forchheimer, 1901), needed at high velocity to model the drag effect on the fluid due to the solid matrix;

- Brinkman extension (Brinkman, 1949), to take into account macroscopic boundary effects.

The Darcy equation and its extensions have been incorporated in the so-called generalized porous medium

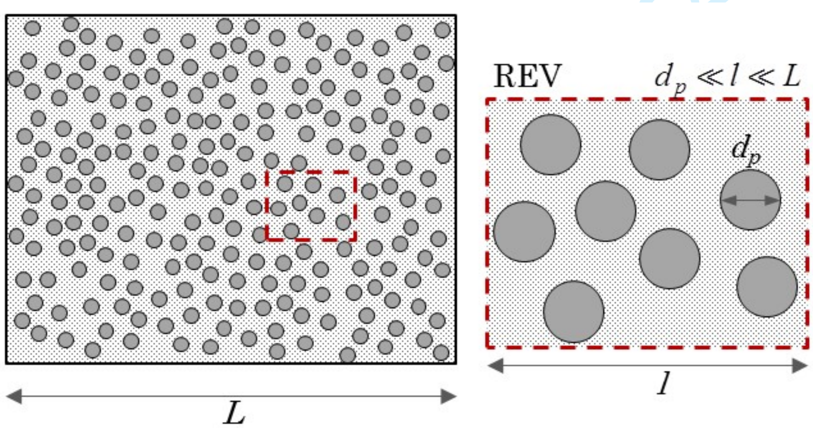

Figure 1: Representative Elementary Volume (REV) and scales in macroscopic approach to model flow in porous media.

model, firstly introduced by Whitaker (1967). This author proposed a volume averaging procedure, later used by Vafai and Tien (1981) and Hsu and Cheng (1990). Based on Whitaker's method, a control volume principle was developed by Nithiarasu et al. (1996) to take into account the variability of porosity in saturated porous media. This generalised model is based on the classical Navier-Stokes equations, to which it approaches when the porosity approaches unity and the permeability tends to infinity.

1.1 Generalized model for porous media in EO

The generalized model for flow through porous media has been used for the first time to investigate EO by Scales and Tait (2006). By using the Navier-Stokes equations, properly averaged to compute flow through porous media (Vafai and Tien, 1981; Liu and Masliyah, 1996; Nithiarasu et al., 1997), they developed a model to describe EO and pressure driven flow in porous media. They introduced an additional term to take into account the effect of charged solid particles, the so-called effective charge density, ρ_{eff}, dependent on the properties of the porous medium. Assuming several simplifying assumptions, they developed the analytical solutions for EOF in porous media for simple geometrical configurations. Kang et al. (2004a) employed the Carman-Kozeny theory (Probstein, 2005) to study Alternating Current (AC) driven EO systems in closed-end micro-channels densely packed with uniform charged spherical micro-particles. They analytically solved the Poisson-Boltzmann equation to derive the internal potential, implemented as a source term in the fluid motion equation. Then they analytically solved the modified Brinkman momentum equation, to calculate the back pressure due to a fixed excitation frequency. As a characteristic length, they used the hydraulic diameter or effective pore diameter. EOF due to AC presents a harmonic sinusoidal oscillation. The oscillating Darcy velocity profile is affected by pore size and excitation frequency. The model developed is validated against experimental results and used to test the effect of several parameters on EOF (Kang et al., 2007). The factors with the largest influence are the ionic concentration and the type of electrolyte, due to their impact on the zeta potential magnitude. On the contrary, the capillary length has a negligible influence. Wall effect is more significant as the ratio between the capillary diameter and the particle diameter decreases. The model has been further extended (Kang et al., 2004b) by distinguishing the contribution from the charged capillary wall and that from charged particles. In the case of neutral packing particles, macroscopic EOF is determined through the Brinkman momentum equation. This latter is modified by implementing the internal potential, introduced as an analytical solution of the Poisson-Boltzmann equation, with channel width used as the reference length. Through this model, Kang et al. (2005) investigated the influence on EOF of the properties of both the working fluid and the porous medium. The effect of charged walls is considerable only in case of similar size of the particles and the micro-capillary. The authors also analysed the effect of the difference between the charge of the wall and that of the particles, founding similar results to those of Liapis and Grimes (2000).

EOF in porous media has been investigated by using the Carman-Kozeny model also by Chai et al. (2007). In particular, they solved the generalized porous medium equations proposed by Nithiarasu et al. (1997) through the Lattice-Boltzmann Method (LBM). They modified the momentum equation to take into account the EO effect by implementing the net charge density, ρ_e, and the effective charge density, ρ_{eff}, into the source term, as proposed by Scales and Tait (2006). The linearized Poisson-Boltzmann equation, averaged through the tortuosity of the porous medium, is used to determine the internal potential. They simulated a micro-channel filled with a solid medium with varying porosity at several operating conditions: generally velocity increases with the applied electric field and the porosity, and decreases as the tortuosity increases, due to the consequent permeability reduction. It also increases with particle size, probably as a consequence of the porosity increase. For larger particle sizes another effect is enhanced: the drag action due to the porous medium prevents the viscous transfer of momentum from the channel walls to the centre of the channel. The velocity near the walls is higher in the case of variable porosity with respect to the condition of constant porosity. As a consequence, porosity variability in the region close to the walls cannot be neglected, confirming the results reported by Cheema et al. (2013).

Recently, the use of non-Newtonian fluids, such as bio-fluids, in EO driven systems is increasing. The generalised model proposed by Nithiarasu et al. (1997) has been used by Tang et al. (2010) to develop a LBM model on the REV scale for EO and pressure driven flow in porous media, with non-Newtonian fluids. Two source terms are added to the momentum equations: one to introduce the flow resistance due to the flow of Non Newtonian fluids in porous media (Herschel and Bulkley, 1926; Al-Fariss and Pinder, 1987) and the other for the electro-kinetic effect. For the EO contribution, charged solid particles and charged channel walls are considered. An effective charge is used to take into account the contribution of porous medium on EOF. A low value of zeta potential is assumed in order to use Debye-Hückel simplification and linearise the Poisson-Boltzmann equation for internal potential computation. A modified zeta potential is considered as a boundary condition to account for the influence of charged solid particles on the internal potential distribution between the parallel walls of the channel. The model developed has been solved through LBM and used to assess the influence of several parameters on EOF. Concerning flow resistance due to the use of non-Newtonian fluids, the velocity increases with decreasing power law exponent and yield stress, and increasing solid particle diameter and porosity. The influence of the channel wall zeta potential is significant close to the wall, whereas the zeta potential of solid particles affects velocity in the central region of the channel.

1.2 Aim of the work

The analysis of available literature on EOF through porous media has highlighted that the existing approaches and models focus on different aspects and that many simplifying assumptions are still used, regarding both electrical field and fluid flow equations (Di Fraia et al., 2018). For this reason, in this work a generalised model is proposed to predict electro-osmotic flow in porous media. As mentioned in the analysis of the state of art (See Section 1), the generalised porous media model has been employed by other authors, especially to derive the analytical solution of simple configurations (Scales and Tait, 2006; Kang et al., 2004a). The computational works in this area appear to have neglected the charge of solid particle inside the porous medium (Kang et al., 2004b, 2005) or ignored the effect of non-linear drag force (the Forchheimer's term in the momentum equation) (Chai et al., 2007).

The proposed model addresses EOF in a comprehensive fashion by

- accounting for the charge of both walls and solid particles;
- including the drag effect on the fluid due to the solid matrix;
- considering the macroscopic boundary effects;
- solving the equations using the Finite Element Method (FEM).

To the best of author's knowledge, a comprehensive FEM model, based on the generalised equations to simulate electro-osmotic flow in porous media is proposed here for the first time. The paper is organised into the following sections. In Section 2 the governing equations of the developed model are introduced. In Section 3, after its verification, the proposed model is used to assess the effectiveness of using porous media to enhance EOF by comparing the results obtained for free channels and channels packed with porous media. Since the literature review has highlighted that many parameters can affect EOF, such comparison is carried out by analysing the influence of channel width, particle size, zeta potential of charged particles and bulk ionic concentration of the electrolyte. Finally, in Section 4, the main conclusions of the work are drawn.

2 Mathematical model and solution procedure

As explained in Section 1, the electric field responsible for EOF is induced by the interaction between an external applied potential and the EDL. The electrokinetic forces responsible for EOF are modelled through a Laplace equation governing the externally applied potential and a Poisson-Boltzmann equation governing the EDL potential. Their effect on the flow is taken into account through a source term in the momentum equation (Patankar and Hu, 1998; Yang and Li, 1998). EOF through porous media is simulated by properly modifying the generalised model for porous media introduced by Nithiarasu et al. (1997) to take into account the charge of both channel walls and porous medium. As mentioned above, this generalised model is based on the classical Navier-Stokes equations, to which it approaches when the porosity approaches unity, and permeability tends to infinity. The equations for EOF are temporally discretized by using the Characteristic Based Split (CBS) algorithm (Nithiarasu, 2003; Nithiarasu et al., 2016), while the Galerkin approximation is used for spatial discretization.

The proposed model is based on the following assumptions:

- 2D modelling, with flat surfaces, characterized by uniform charge along their length;
- Boltzmann distribution for the ions inside the electrolyte;
- constant properties of the electrolyte;
- incompressible fluid;
- constant porosity;

- steady and fully developed flow.

2.1 Governing equations

The external potential ϕ is governed by a Laplace equation of the type:

$$\sigma_p \frac{\partial^2 \phi}{\partial x_i^2} = 0 \tag{1}$$

where σ_p is the electrical conductivity of porous medium particles. The external electric field, E_x, and the external electric potential, ϕ, are related via

$$E_x = -\frac{\partial \phi}{\partial x_i} \tag{2}$$

The EDL potential, ψ, is described by a Poisson-Boltzmann equation, as follows:

$$\frac{\partial^2 \psi}{\partial x_i^2} = -\frac{\rho_e}{\varepsilon \varepsilon_0} \tag{3}$$

where ε is the dielectric constant of the electrolyte, ε_0 is the permittivity of vacuum and ρ_e is the net charge density.

The equilibrium Boltzmann distribution equation can be used to predict the ionic number concentration in the case of fully developed flow with small Peclet numbers (Yang et al., 2001) and in the absence of overlapping of EDLs (Qu and Li, 2000). The ions in the solution are assumed to be equal but opposite in charge, and they are related to their energy $(ze\psi)$ as

$$n^+ = n_0 \exp\left(-\frac{ze\psi}{k_{Bo}T}\right); \qquad n^- = n_0 \exp\left(\frac{ze\psi}{k_{Bo}T}\right); \tag{4}$$

where n^+ and n^- represent the number of positive and negative ions, respectively, n_0 is the ionic number concentration in the bulk solution, z is the valance of the ions, e is the elementary charge, k_{Bo} is the Boltzmann's constant and T is the temperature in kelvin. The bulk ionic concentration n_0 can be obtained as

$$n_0 = cN_A \tag{5}$$

where c is the concentration of the electrolyte in Moles and N_A is Avogadro constant. Therefore, the net charge density can be defined as

$$\rho_e = ze\left(n^+ - n^-\right) \tag{6}$$

Using hyperbolic functions, the net charge density can be expressed as

$$\rho_e = -2n_0 ze \sinh\left(\frac{ze\psi}{k_{Bo}T}\right) \tag{7}$$

The non-linear Poisson-Boltzmann equation, obtained by substituting Equation 7 into Equation 3, allows to determine the internal potential distribution of the ions inside the fluid as

$$\frac{\partial^2 \psi}{\partial x_i^2} = \frac{2n_0 ze}{\varepsilon\varepsilon_0} \sinh\left(\frac{ze\psi}{k_{Bo}T}\right) \tag{8}$$

Fluid flow phenomena through porous media due to EO is modelled by using the modified generalised model for porous media, that can be written as follows.

- Continuity equation

$$\frac{\partial \rho_f}{\partial t} + \rho_f \frac{\partial \bar{u}_i}{\partial x_i} = 0 \tag{9}$$

where ρ_f the fluid density, and $\bar{u}_i$ is the volume averaged velocity defined as a function of the fluid velocity, u_i, $\bar{u}_i = \Phi u_i$, in which Φ is the medium porosity. By using the ideal gas law, the speed of sound c can be expressed as

$$c^2 = \frac{\partial p}{\partial \rho_f} \tag{10}$$

where p is the pressure. The continuity equation can be rewritten as follows

$$\frac{1}{c^2}\frac{\partial p}{\partial t} = -\rho_f \frac{\partial \bar{u}_i}{\partial x_i} \tag{11}$$

For incompressible flows, the speed of sound may be replaced with an artificial compressibility parameter β, (Nithiarasu, 2003).

- Momentum equation

$$\frac{\rho_f}{\Phi}\left(\frac{\partial \bar{u}_i}{\partial t} + \frac{\partial}{\partial x_j}\frac{(\bar{u}_i \bar{u}_j)}{\Phi}\right) = -\frac{1}{\Phi}\frac{\partial \Phi p}{\partial x_i} + \frac{\mu_{eff}}{\Phi}\frac{\partial^2 \bar{u}_i}{\partial x_i^2} - \frac{\mu_f}{K}u_i - \rho_f \frac{c_F}{\sqrt{K}}|\mathbf{V}|\bar{u}_i + \Phi(\rho_e + \rho_{eff})E_x \tag{12}$$

where μ_{eff} is the effective viscosity, used to take into account the viscous effect that increases as porosity and permeability increase (Massarotti et al., 2003), μ_f is the fluid viscosity, $\mathbf{V}$ is the velocity vector in the porous medium. The medium permeability K takes the well-known form of (Vafai, 2005)

$$K = \frac{\Phi^3 d_p^2}{b(1-\Phi)^2} \tag{13}$$

and the Forchheimer coefficient c_F is given as (Ergun and Orning, 1949)

$$c_F = \frac{b}{\sqrt{d\Phi^3}} \tag{14}$$

where constants b and d $(b = 150, d = 1.75)$ depend on the microscopic geometry of the porous medium and d_p is the particle size of the bed.

The last term of Equation (12) takes into account the driving force of EOF due to the interaction between the EDL potential of both channel walls and particles composing the porous medium, and the external electric field. The effective charge density, ρ_{eff}, is added to the net charge density, ρ_e, in the source term, as proposed by Tang et al. (2010). Considering a cylindrical pore, an analytical expression may be expressed for effective charge density as (Tang et al., 2010):

$$\rho_{eff} = \frac{\Phi\varepsilon\varepsilon_0\zeta_p}{K}\left(\frac{2I_1(\kappa R_{pore})}{\kappa R_{pore} I_0(\kappa R_{pore})} - 1\right) \tag{15}$$

where I_n is the modified Bessel function of the first type of order n and R_{pore} is the average pore size calculated as

$$R_{pore} = \frac{d_p\Phi}{3(1-\Phi)} \tag{16}$$

The generalised model equations (Equations (11) and (12)) discussed above reduce to the Navier Stokes equations when the solid matrix in the porous medium disappears, i.e. when Φ tends to 1. Writing Equation (12) as

$$\frac{\rho_f}{\Phi}\left(\frac{\partial \bar{u}_i}{\partial t} + \frac{\partial}{\partial x_j}\frac{(\bar{u}_i\bar{u}_j)}{\Phi}\right) = -\frac{1}{\Phi}\frac{\partial \Phi p}{\partial x_i} + \frac{\mu_{eff}}{\Phi}\frac{\partial^2 \bar{u}_i}{\partial x_i^2} - P \tag{17}$$

where

$$P = \frac{\mu_f}{K}u_i + \rho_f\frac{c_F}{\sqrt{K}}|\mathbf{V}|\bar{u}_i + \Phi(\rho_e + \rho_{eff})E_x \tag{18}$$

the same set of equations described above can be used to analyse the case of single-phase fluid, by assuming that the porosity is 1 and the term P is 0.

2.1.1 Dimensionless form of the governing equations

For a homogeneous medium, with constant, uniform porosity and constant properties, the dimensionless form of the governing equations described above can be obtained through the following non-dimensional scales:

$$x_i^* = \frac{x_i}{L_{ref}}; \qquad \phi^* = \frac{ze\phi}{k_{Bo}T}; \qquad \psi^* = \frac{ze\psi}{k_{Bo}T}; \qquad \rho^* = \frac{\rho_f}{\rho_{ref}}; \qquad u_i^* = \frac{u_i}{u_{ref}};$$

$$u_{ref} = \frac{E_x\varepsilon\varepsilon_0\zeta}{\mu_f}; \qquad t^* = \frac{tu_{ref}}{L_{ref}}; \qquad p^* = \frac{p-p_{ref}}{\rho_{ref}u_{ref}^2}; \qquad \sigma^* = \frac{\sigma}{\sigma_{ref}}$$

where the subscript *ref* indicates a reference value and ζ is the zeta potential.

- *Laplace equation*

$$\sigma^*\frac{\partial^2\phi^*}{\partial x_i^{*2}} = 0 \tag{19}$$

where

$$\sigma^* = \frac{\sigma_p}{\sigma_{ref}}$$

- *Poisson-Boltzmann equation*

$$\frac{\partial^2\psi^*}{\partial x_i^{*2}} = -\left(\kappa L_{ref}\right)^2\sinh\left(\psi^*\right) \tag{20}$$

where κ^{-1} is known as Debye length and corresponds to the EDL characteristic thickness (Patankar and Hu, 1998)

$$\kappa^{-1} = \left(\frac{k_{Bo}T\varepsilon\varepsilon_0}{2n_0z^2e^2}\right)^{1/2}$$

and the reference length, L_{ref}, corresponds to the channel width.

- *Continuity equation*

$$\frac{1}{\beta^{*2}}\frac{\partial p^*}{\partial t^*} = -\rho^*\frac{\partial\bar{u}_i^*}{\partial x_i^*} \tag{21}$$

where the artificial compressibility parameter, β, (Nithiarasu, 2003) is locally calculated at each node as (Massarotti et al., 2006):

$$\beta = \max\left(\eta, u_{conv}, u_{diff}\right) \tag{22}$$

The constant η is assumed to be 0.5, u_{conv} and u_{diff} are the convective and diffusive velocities, respectively.

- *Momentum equation*

$$\frac{\rho^*}{\Phi}\left(\frac{\partial \bar{u}_i^*}{\partial t^*}+\frac{1}{\Phi}\frac{\partial\left(\bar{u}_i^*\bar{u}_j^*\right)}{\partial x_j^*}\right)=-\frac{\partial p^*}{\partial x_i^*}+\frac{1}{\Phi Re}\frac{\partial^2\bar{u}_i^*}{\partial x_i^{*2}}-\frac{1}{ReDa}\bar{u}_i^*-\frac{c_F}{Da^{1/2}}|\mathbf{V}|\,\bar{u}_i^*$$
$$+\Phi(J\sinh(\psi^*)+J_{eff})\left(-\frac{\partial\phi^*}{\partial x_i^*}\right) \tag{23}$$

where

$$Re=\frac{\rho_{ref}u_{ref}L_{ref}}{\mu_f}=\rho_{ref}\left(\frac{E_x\varepsilon\varepsilon_0\zeta}{\mu_f}\right)\left(\frac{L_{ref}}{\mu_f}\right)\qquad Da=\frac{K}{L_{ref}^2};$$

$$J=\frac{2n_0k_{Bo}T}{u_{ref}^2\rho_{ref}}\qquad J_{eff}=\frac{\Phi\varepsilon\varepsilon_0\zeta_p}{K}\frac{k_{Bo}T}{zeu_{ref}^2\rho_{ref}}\left(\frac{2I_1(\kappa R_{pore})}{\kappa R_{pore}I_0(\kappa R_{pore})}-1\right) \tag{24}$$

From here onwards the volume averaged components of velocity will be indicated as u_i instead of $\bar{u}_i$, for the sake of simplicity.

The above set of non-dimensional equations has been solved by using fully explicit artificial compressibility-based CBS scheme (Nithiarasu, 2003; Nithiarasu et al., 2016).

2.1.2 *Boundary and Initial Conditions*

The layout of the micro-channel considered in this work is shown in Figure 2, with the boundary conditions applied.

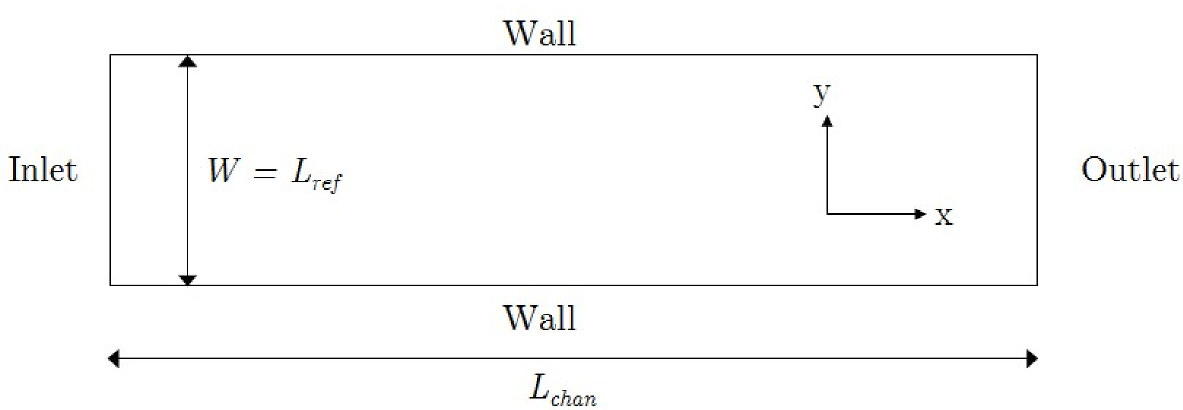

Figure 2: Rectangular 2D micro-channel considered in the simulations.

An external potential difference between the inlet and outlet, $\phi_1^*-\phi_2^*$, is considered to be applied, and the normal components of velocity gradients are assumed to be zero at both inlet and outlet.

$$at: x=0\qquad \frac{\partial\psi^*}{\partial x^*}=0;\qquad \phi^*=\phi_1^*;\qquad \frac{\partial u_i^*}{\partial x^*}=0;$$
$$at: x=L_{chan}\qquad \frac{\partial\psi^*}{\partial x^*}=0;\qquad \phi^*=\phi_2^*;\qquad \frac{\partial u_i^*}{\partial x^*}=0; \tag{25}$$

The channel walls are assumed to be active with a prescribed non-dimensional modified zeta potential, $\zeta_w^{'}$, and to obey no-slip velocity boundary conditions; the external potential gradient in y direction is equal to zero:

$$\psi^* = \zeta_w^{'}; \qquad \frac{\partial \phi^*}{\partial y^*} = 0; \qquad u_1^* = 0 \tag{26}$$

$\zeta_w^{'}$ is considered to take into account the effect of charged solid particles on internal potential distribution within the micro-channel (Tang et al., 2010) and the possible overlap between the internal potential of particles and channel walls (Scales and Tait, 2006). Considering the linearized Poisson-Boltzmann equation, the model proposed by Rice and Whitehead (1965) is used to define the modified wall zeta potential (Rice and Whitehead, 1965) as:

$$\zeta_w^{'} = \zeta_p \left(1 - \frac{2I_1(\kappa R_{pore})}{\kappa R_{pore} I_0(\kappa R_{pore})}\right) + \zeta_w - \zeta_p \tag{27}$$

where ζ_p is the zeta potential of the porous material.
The computation is started with prescribed zero velocity components as the initial condition.

3 Results and discussions

The proposed numerical model is used to investigate EO in free channels and channels packed with porous media, in order to assess the effectiveness of using porous media to enhance EOF.
A silicon micro-channel of 30 μm in width, characterized by an aspect ratio of 10, with deionized water as working fluid is considered as a reference case study. The electrical conductivity, σ_p, and dynamic viscosity, μ_f, are assumed to be constant. The zeta potential acting on channel walls and, in case of EOF through porous media, on the boundaries of the solid particles, is assumed to be equal to -19 mV. This value corresponds to a modified zeta potential equal to -15 mV (see Equation 27). The value considered for the zeta potential imposed on the charged surfaces is derived from some experimental investigations carried out on electro-osmotic flow in silicon microchannels (Eng and Nithiarasu, 2009). An external electric field of 1 kV/m is applied. The other parameters used in this study are reported in Table 1.

Table 1: Parameters used in the numerical simulations.

Parameter	Measurement unit	Value
Dielectric constant of the electrolyte, ε	78.4	-
Permittivity of vacuum, ε_0	$8.85 \cdot 10^{-12}$	$C \cdot (V \cdot m)^{-1}$
Ionic concentration in the bulk solution, n_0	$6.022 \cdot 10^{+19}$	m^{-3}
Valence of the ions, z	1	-
Elementary charge, e	$1.602 \cdot 10^{-19}$	C
Boltzmann constant, k_{Bo}	$1.381 \cdot 10^{-23}$	$m^2 kg \cdot (s^2 K)^{-1}$
Temperature, T	298	K
Fluid density, ρ	1000	$kg \cdot m^{-3}$
Fluid viscosity, μ	$8.91 \cdot 10^{-4}$	$Pa \cdot s$

In channels packed with porous media, a porosity equal to 0.8 is assumed. The porous medium is composed of silicon circular particles with a diameter equal to 16% of the channel width.

A set of 2D unstructured meshes, refined near all the solid boundaries to capture the rapid change in both internal potential and velocity, is used. The details of the meshes used for plain channels and channels with obstructions are shown in Figure 3. A mesh sensitivity study has been carried out to finalise the meshes used in the calculations.

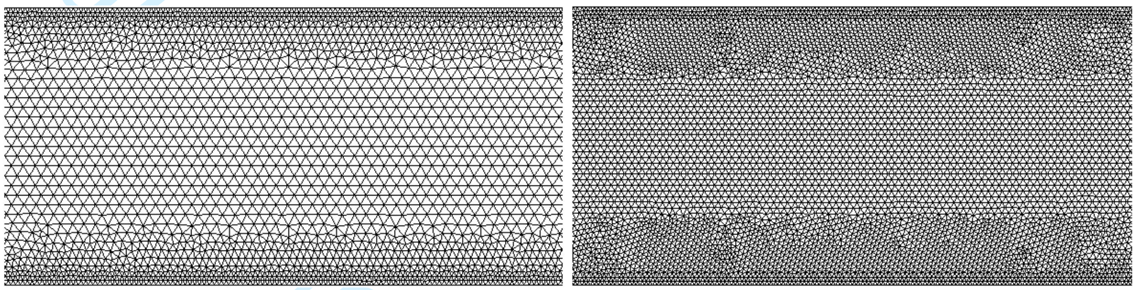

(a) Free channel. (b) Porous medium channel.

Figure 3: Meshes of micro-channels considered in the simulations.

3.1 Verification of the model

The numerical model described in Section 2 is used to determine EOF in free channels and channels packed with porous media. The results are compared to the available analytical solutions.

For a two dimensional rectangular channel, the analytical solution for the internal potential in free channels can be written as (Patankar and Hu, 1998):

$$\psi = \frac{\cosh\left[\kappa W\left(y - 1/2\right)\right]}{\cosh\left[\kappa W/2\right]} \tag{28}$$

where y is the distance from the wall and W is the channel width. The analytical solution for the horizontal velocity component in free channels (Arnold, 2007) may be expressed as:

$$u = 1 - \zeta\left(2\ln\frac{1+\exp\left(-\kappa W y\right)\tanh\left(\frac{1}{4}\zeta_w\right)}{1-\exp\left(-\kappa W y\right)\tanh\left(\frac{1}{4}\zeta_w\right)}\right) \tag{29}$$

In Figure 4, the internal potential and velocity profiles in free channels are plotted. In all plots, the quantities are non-dimensional, and half width of the channel is considered for the sake of clarity.

Since the analytical solution is derived for the linearized Poisson-Boltzmann equation, there is a slight discrepancy between the analytical solution and the numerical results. The data of the simulations for velocity are normalised against the maximum velocity in order to have a clear comparison with the analytical solution.

For EOF in channels packed with porous media, Scales and Tait proposed different analytical solutions (Scales and Tait, 2006). For EOF between two parallel plates in a porous channel of width W, with a

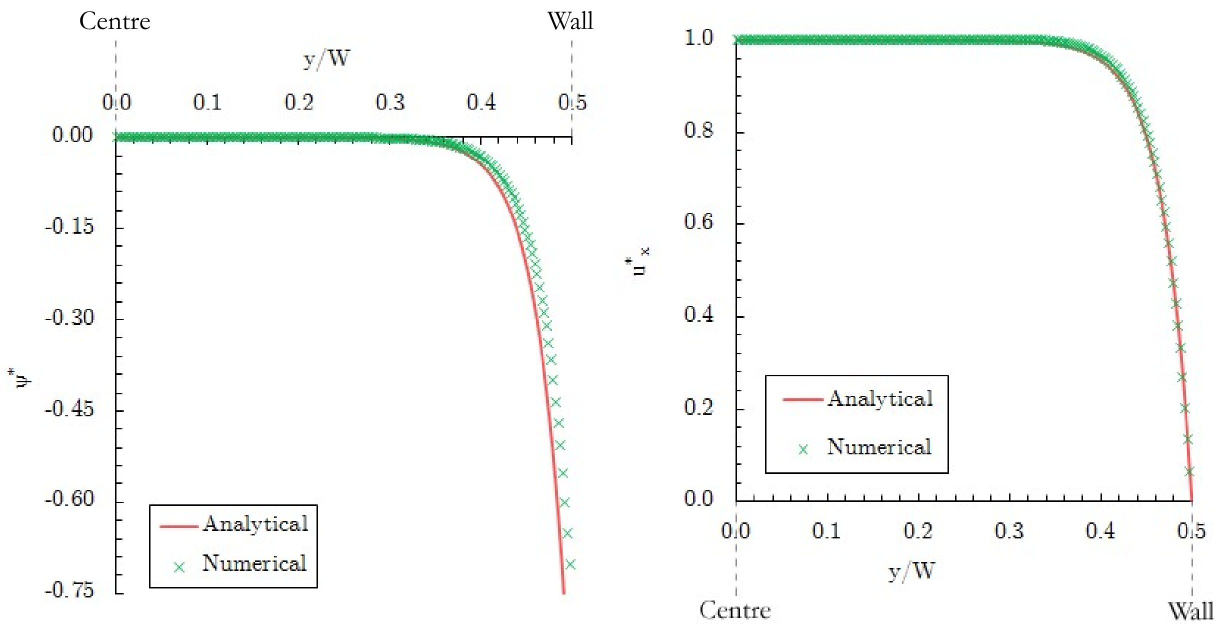

(a) Internal potential profile. (b) Horizontal velocity profile.

Figure 4: Comparison of the present results with analytical solutions in free channels for the reference case study. Half width of the channel is plotted for the sake of clarity.

modified zeta potential ζ_w' applied at the channel walls, the solution to the linearized Poisson-Boltzmann equation can be expressed as:

$$\psi(y) = \left(\zeta_w' \frac{sinh\left(\sqrt{\tau}\kappa y\right)}{sinh\left(\sqrt{\tau}\kappa W\right)} + \zeta_w' \frac{sinh\left(\sqrt{\tau}\kappa (c-y)\right)}{sinh\left(\sqrt{\tau}\kappa W\right)} \right) \tag{30}$$

In the analysed case, the tortuosity, τ is assumed to be equal to 1. For the horizontal velocity two different cases can be analysed:

- uncharged walls and charged porous medium ($\zeta_w = 0$)

$$\bar{u}(y) = \bar{u}_d \left(1 - \frac{e^{-\lambda(W-y)} - e^{-\lambda(2W-y)} + \left(1 - e^{-\lambda W}\right) e^{-\lambda y}}{1 - e^{-\lambda 2W}} \right) \tag{31}$$

where $\bar{u}_d$ is given by the Darcy's law, as

$$\bar{u}_d = -\frac{K}{\sqrt{\tau}\mu_{eff}} \left(\nabla p + \rho_{eff} \nabla \phi \right) \tag{32}$$

and λ is the Brinkmann screening length defined as

$$\lambda = \sqrt{\frac{\Phi\sqrt{\tau}}{K} \frac{\mu_{eff}}{\mu_f}} \tag{33}$$

- charged walls and uncharged porous medium ($\zeta_p = 0$)

$$\bar{u}(y) = Z\left(\frac{\psi_{w1}\left(e^{-\lambda(2W-y)} - e^{-\lambda y}\right) + \psi_{w2}\left(e^{-\lambda(W+y)} - e^{-\lambda(W-y)}\right)}{1 - e^{-\lambda 2W}}\right) + Z\psi(y) = Zu_B(y) + Z\psi(y) \tag{34}$$

$$Z = \frac{\varepsilon\varepsilon_0\kappa^2\nabla\phi}{\mu_f(\lambda^2 - \tau\kappa^2)} \tag{35}$$

The superposition of the individual cases, Eq.s (31) and (34), is used to analyse the case of charged walls and charged porous medium.

In Figure 5, the profiles of internal potential and velocity, in the case of EOF through porous media, are plotted and compared to their analytical solution. A good agreement between the results of the proposed algorithm and the analytical solutions is found. The internal potential profile is similar in shape to that obtained for free channels (see Figure 4a), but different in magnitude since the modified zeta potential is applied on channel walls. A slight increase of the horizontal velocity can be observed in the region close to the channel walls. The analytical solutions proposed by Scales and Tait (2006) are also used to determine

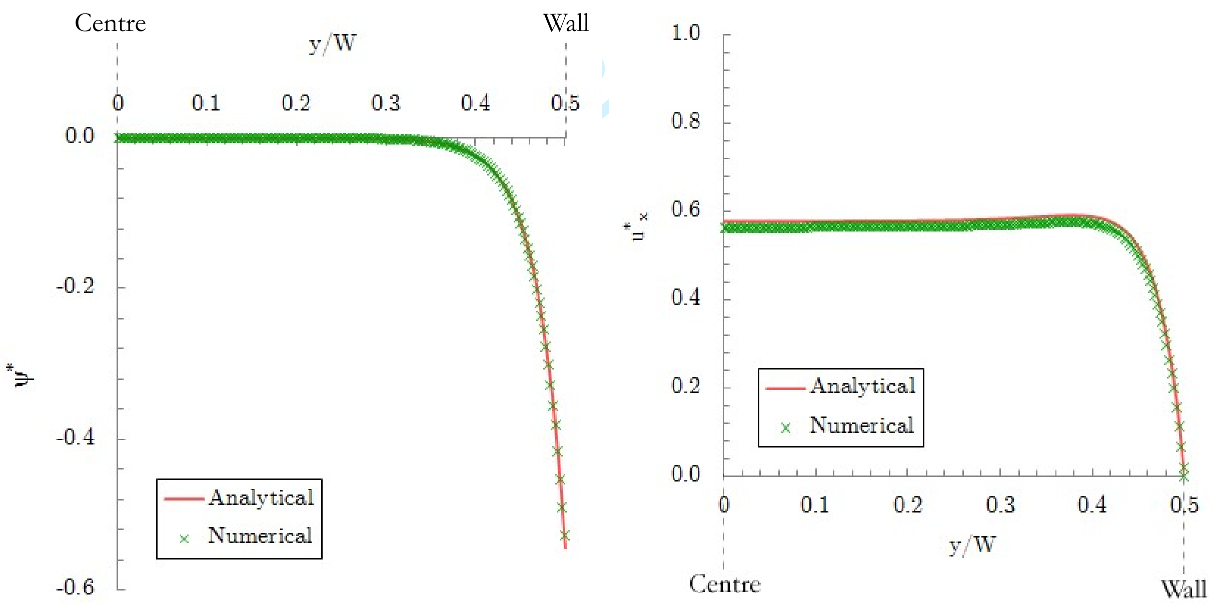

(a) Internal potential profile.

(b) Horizontal velocity profile.

Figure 5: Comparison of results from numerical simulations against analytical solutions in channels packed with porous media for the reference case study. Half width of the channel is plotted for the sake of clarity.

EO velocity in case of charged particles with neutral walls, u^*_{cp}, (Figure 6a), and for charged walls with neutral particles, u^*_{cw}, (Figure 6b), in order to assess the influence of charged particles and of charged walls on EOF. The average velocity is significantly higher in the case of charged particles and neutral walls, u^*_{cp}, than in the case of charged walls and neutral particles, u^*_{cw}.

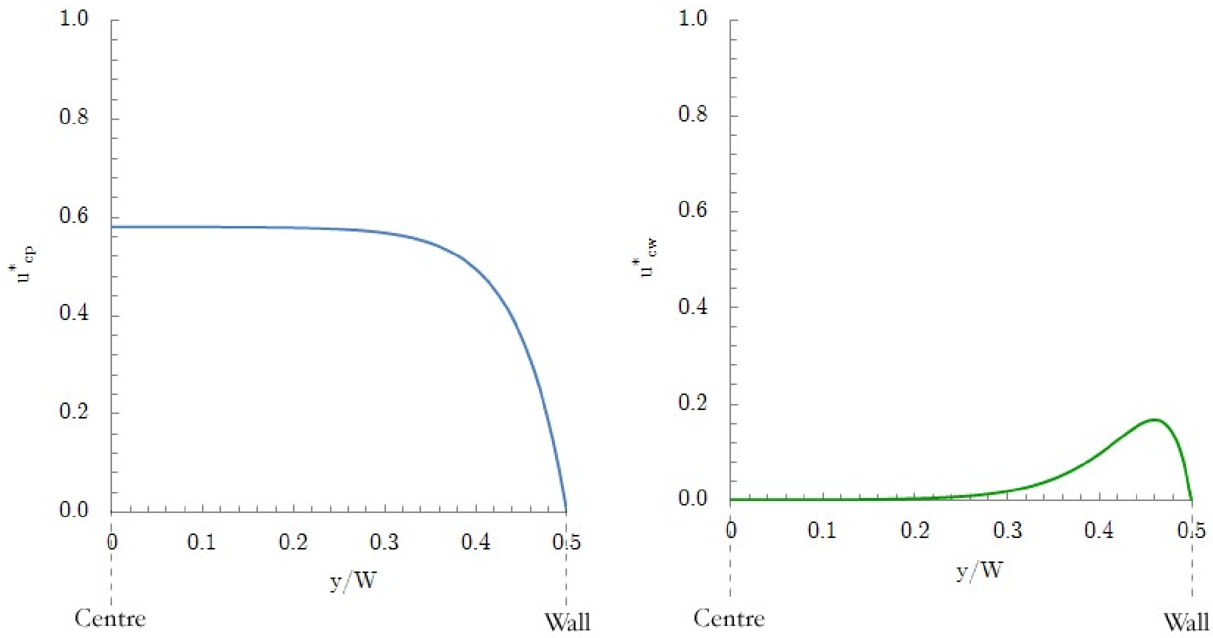

(a) Charged particles and neutral walls. (b) Charged walls and neutral particles.

Figure 6: Horizontal velocity profile. Half width of the channel is plotted for the sake of clarity.

Two important conclusions can be drawn from this analysis:

- solid charged particles have a strong influence on EOF driven systems;
- neglecting the effect of charged media in micro-channels on EOF, as done in many previous works concerning EOF through porous media, can have a strong influence on the solution of the model.

3.2 *Sensitivity analyses*

The effect of several parameters on EOF through porous media is investigated in order to find optimal values for the flow. To this aim, the parameters governing electro-kinetic phenomena responsible for fluid flow are analysed through the algorithm for EOF based on the generalized model for porous media flow.

3.2.1 *Effect of micro-channel width on EOF*

The geometry of the micro-channel significantly influences EOF. For this reason, this parameter is investigated, comparing its effect in free channels and channels packed with porous media. A range of different channel widths, W, between $5\mu m$ and $150\mu m$, is considered. The profiles of internal potential and horizontal velocity at the outlet section of the channel are reported for different channel widths in Figures 7 and 8, respectively.

In both cases, as the channel width increases, the internal potential presents higher gradients close to the

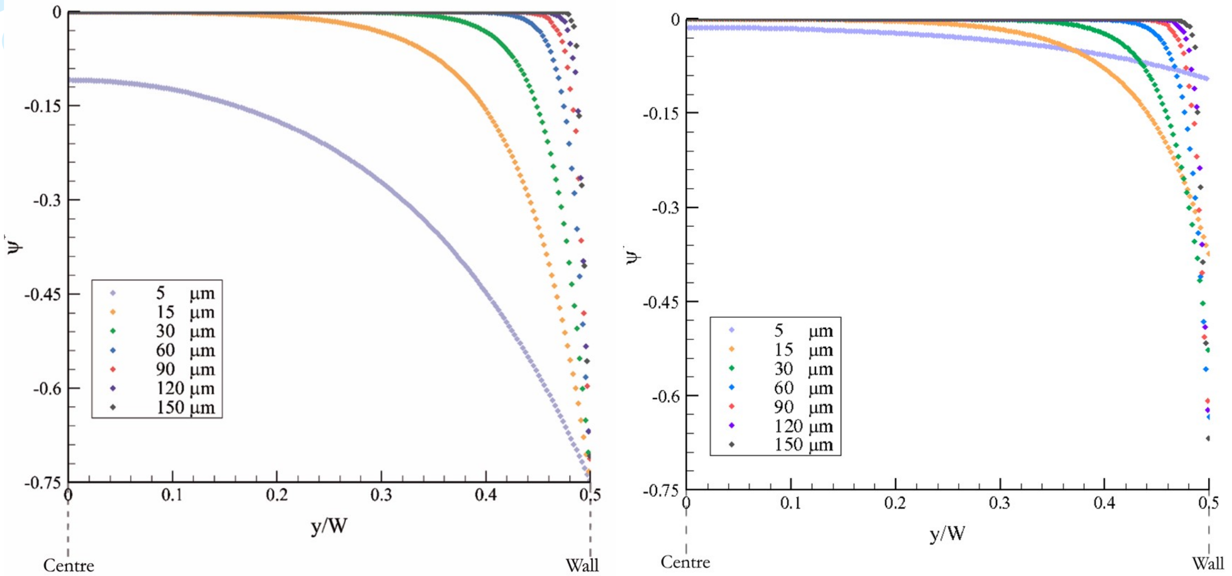

(a) Free channel. (b) Porous media channel.

Figure 7: Internal potential at different channel widths.

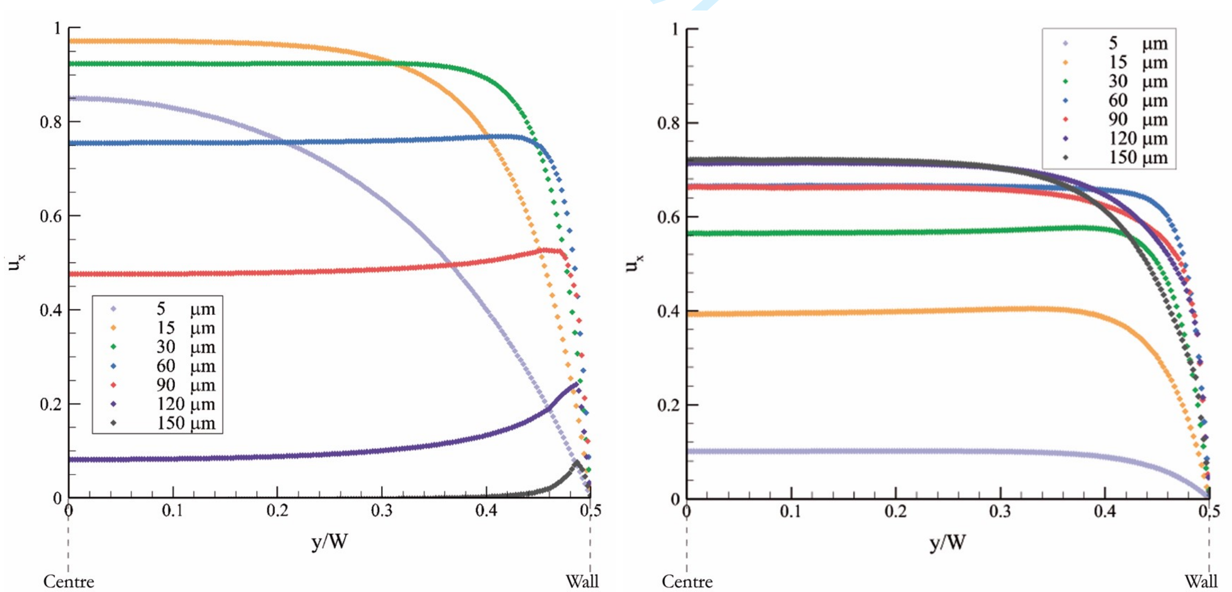

(a) Free channel. (b) Porous media channel.

Figure 8: Horizontal velocity at different channel widths.

channel walls and goes to zero in the central region of the channel. This behaviour is weaker in porous media channels, where the charge of the particles balances the increase of width effect. In the case of free channel the zeta potential applied on the channel walls does not vary with the channel width. In channels packed with porous media, the zeta potential, imposed as a boundary condition on the channel walls for internal potential, varies with porosity and particle size. In the current analysis the porosity is constant and assumed equal to 0.8, whereas the particle diameter varies with the channel width. As the channel width increases, the particle diameter increases and then the magnitude of the zeta potential and the maximum internal potential increase. However, the modified zeta potential, used in the case of porous media channel, is always lower than the zeta potential really acting on channel walls and used for the simulation of the free channels. For the sake of clarity, the values of modified zeta potential at different channel widths are reported in Table 2. It is important to remember that the zeta potential acting on the channel walls is equal to -19 mV.

Table 2: Modified zeta potential, ζ_w', calculated for different values of channel width.

Channel width W μm	Modified zeta potential ζ_w' mV
5	-2.45
15	-9.63
30	-13.9
60	-16.5
90	-17.4
120	-17.8
150	-18.1

The internal potential significantly influences EO velocity. In the free channel, the average velocity increases with the channel width in a very small range of micro-channel widths, from *5* to $15\mu m$, while beyond this value it rapidly decreases (See Figure 8a). This is due to the increase in the distance between the channel walls that lowers the effect of the EDL potential, reducing the average velocity. For this reason, EO flow in free channel is applied only at micro scale. As shown in Figure 8b, in porous media channels the average velocity rapidly increases in the same rage of channel width (from *5* to $15\mu m$), but it is lower than in free channels. This is due to the modest value of zeta potential applied on the channel walls, and to the small distance between particles, that causes higher resistance to fluid flow. The higher the channel width, the higher the average velocity. Beyond $60\mu m$, the velocity is higher than in free channels. Moreover, beyond this value the influence of the charge of channel walls decreases and EOF is mainly due to the charge of solid particles. In fact, the velocity profile approaches that observed in the case of charged particles and uncharged walls (See Figure 6a). As the channel width further increases, the variability of average velocity with channel width tends to decrease.

The results in terms of flow rate are reported in Table 3, together with the results obtained for the free channel.

Table 3: Flow rate for different micro-channel widths with and without porous media.

Channel width μm	Flow rate in micro-channel packed with porous media $\mu m^2 min^{-1}$	Flow rate in free channel $\mu m^2 min^{-1}$
5	$3.63 \cdot 10^{-4}$	$2.87 \cdot 10^{-3}$
15	$4.57 \cdot 10^{-3}$	$1.18 \cdot 10^{-2}$
30	$1.48 \cdot 10^{-2}$	$2.41 \cdot 10^{-2}$
60	$3.26 \cdot 10^{-2}$	$4.10 \cdot 10^{-2}$
90	$4.84 \cdot 10^{-2}$	$4.01 \cdot 10^{-2}$
120	$5.91 \cdot 10^{-2}$	$1.21 \cdot 10^{-2}$
150	$6.31 \cdot 10^{-2}$	$2.32 \cdot 10^{-4}$
180	$1.09 \cdot 10^{-1}$	-
210	$1.28 \cdot 10^{-1}$	-
240	$1.47 \cdot 10^{-1}$	-

The analysis confirms the efficacy of EO to drive flow through porous media. It is worth to notice that, contrary to what happens in free channels, the flow rate through porous media increases in the whole range of channel widths analysed. As mentioned above, for larger channel widths, EO is mainly affected by the charge of solid particles, rather than that of channel walls. For this reason, EO can be effectively used to drive flow through porous media independently on the scale of the system, contrary to what happens in free fluid systems, where the efficiency of EO as driving force becomes negligible as the scale of the system increases.

3.2.2 Effect of solid particle diameters on EOF

Several parameters depend on the diameter of solid particles. It affects the hydraulic radius, Eq. (16), and, as a consequence, the modified zeta potential applied on the channel walls, Eq. (27), and the non dimensional parameter that takes into account the effect of charged solid particles on EOF, Eq. (24). Moreover, the solid particle diameter influences the permeability of the porous medium, Eq. (13), and, therefore, the fluid velocity. The reference case (P16% from now on) is simulated by varying the diameter of solid particles, that is here assumed equal to 12% (P12% from now on) and 29% (P29% from now on) of the channel width, by keeping constant the porosity. The horizontal velocity profiles for the particle sizes considered are shown in Figure 9.

The average velocity is higher when the porous medium is made of larger particles, with a higher difference at smaller channel widths. In the range between *5* and 30μm), also the rate of increase of the average velocity is higher in P29% than in P16%. These trends appear to be affected by the modified zeta potential, applied as a boundary condition on channel walls, and the permeability. As shown in Fig. 10, the higher the particle size, the higher the zeta potential in absolute value and the permeability of the porous medium.

This could explain the higher velocities found for larger particles. Smaller the channel width, smaller the

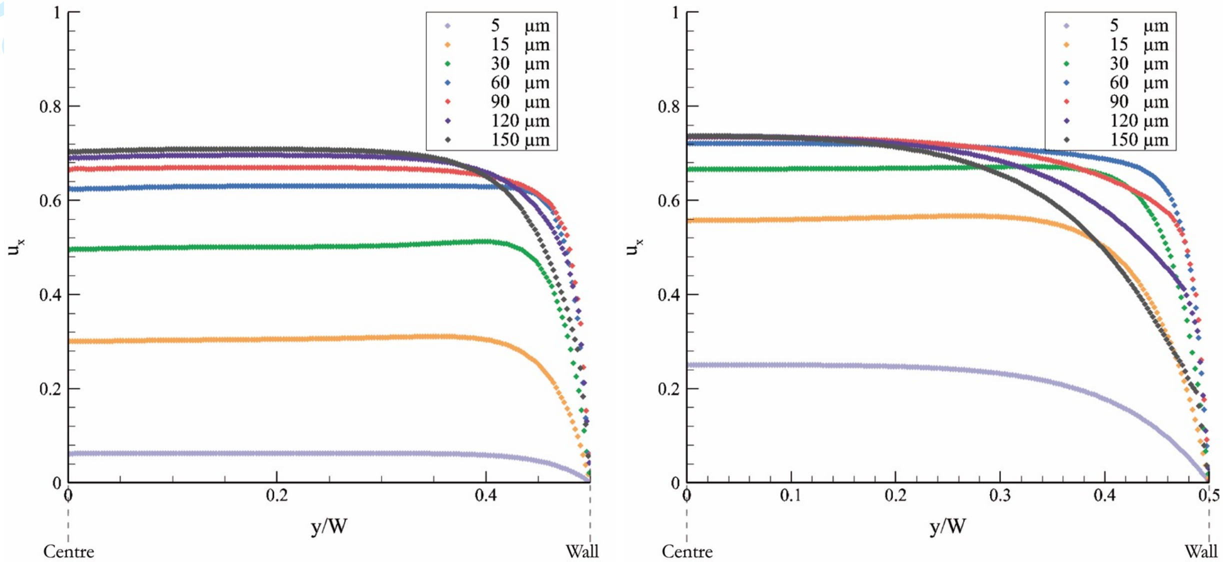

(a) P12%. (b) P29%.

Figure 9: EO velocity at different particles sizes plotted at different channel widths.

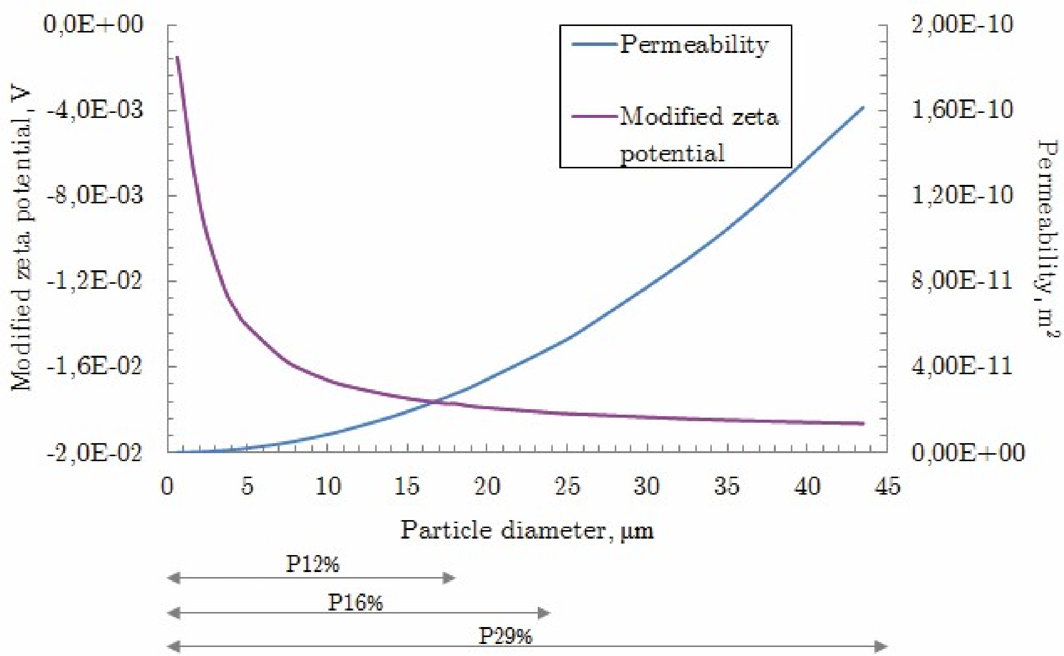

Figure 10: Variability of modified zeta potential and permeability with particle diameter. The range of the three cases analysed, P12%, P16% and P29%, is shown for the sake of clarity.

particle size: in the lower range of channel widths, the higher difference between the two cases can be explained considering the fast growth in absolute value of the modified zeta potential. The use of larger particles reduces the increase of velocity near the walls; in both cases it further decreases as the channel width is larger than $90\mu m$. Beyond this value, the velocity profile tends to that obtained in case of charged particles and uncharged walls (See Figure6a), indicating a strong influence of the charge of solid particles. At the upper bound of the range considered for the channel width, the difference in maximum velocity decreases for the two cases analysed. This aspect is more evident in Fig. 11, where all of the particle sizes analysed are compared in terms of flow rate.

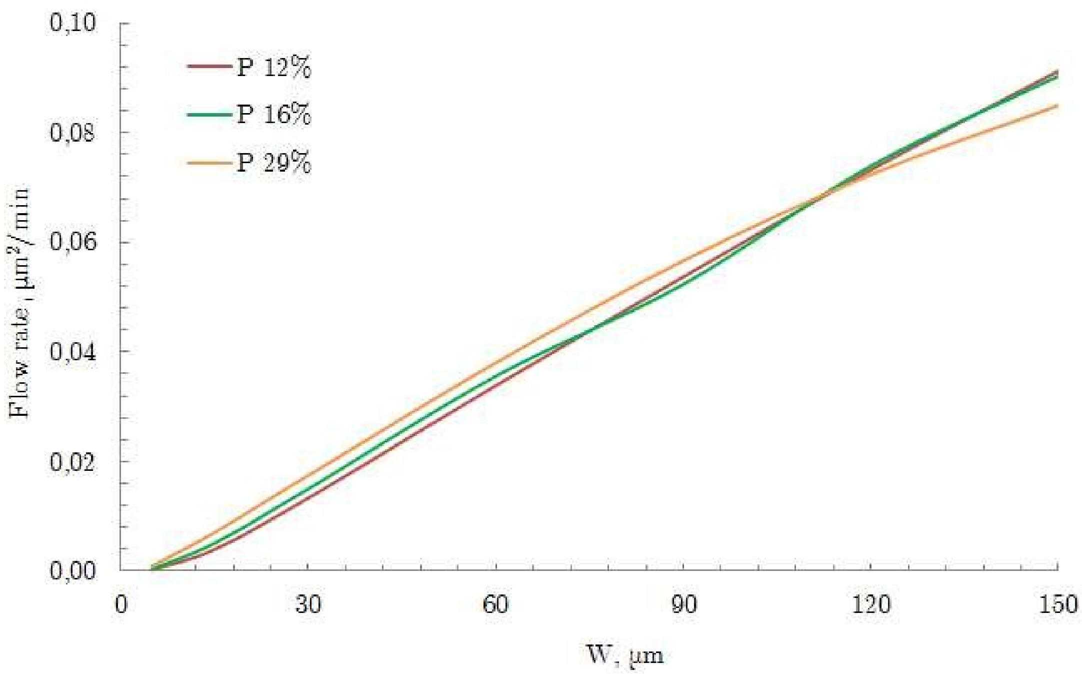

Figure 11: Flow rate at different widths of micro-channels with varying particle diameter.

In the case of smaller particles (P12%), the trend is very similar to that of the reference case (P16%). It is worth noticing that, the flow rate grows with particle size, up to a channel width equal to roughly $110\mu m$, whereas beyond this value the use of larger particles produces lower flow rate, even though their use enhances permeability. In this last case, the flow rate even decreases as the channel width exceeds $120\mu m$. This can be explained by considering the internal potential and horizontal velocity distributions within the channel, illustrated in Fig. 12. The thickness of EDL is the same for both the particles sizes analysed at the same channel width, as shown in Figures 12a and 12b, 12c and 12d. The difference is in the magnitude of internal potential: as mentioned above, a higher zeta potential in absolute value is imposed in case of larger particles and this increases the internal potential near the walls. As shown in Figure 10, such an increase is considerable up to a particle size of 10 μm, whereas beyond this value the trend is approximately constant. For this reason, the distributions shown in Figures 12c and 12d, corresponding to a particle diameter equal to 14 and 35 μm, respectively, are similar. In terms of velocity, the difference between the cases taken into account is more significant. In channels of 30 μm in width, a substantial decrease in velocity can be

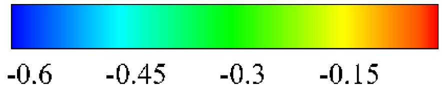

(a) P12%, channel width equal to 30 μm.

(b) P29%, channel width equal to 30 μm.

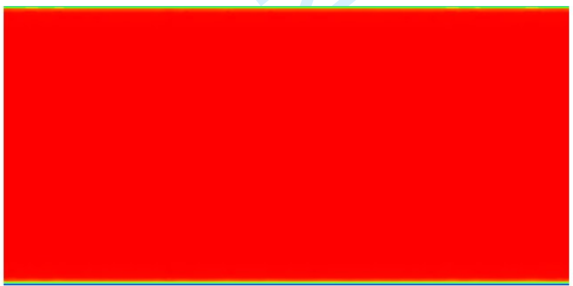

(c) P12%, channel width equal to 120 μm.

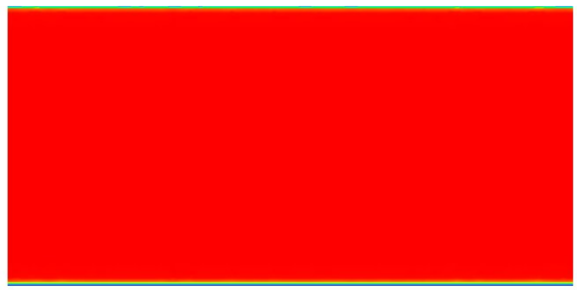

(d) P29%, channel width equal to 120 μm.

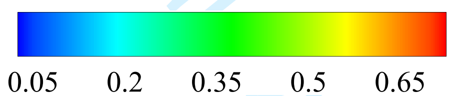

(e) P12%, channel width equal to 30 μm.

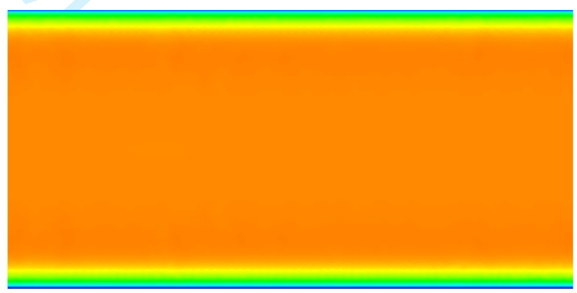

(f) P29%, channel width equal to 30 μm.

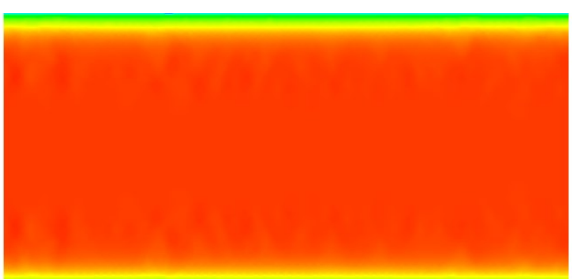

(g) P12%, channel width equal to 120 μm.

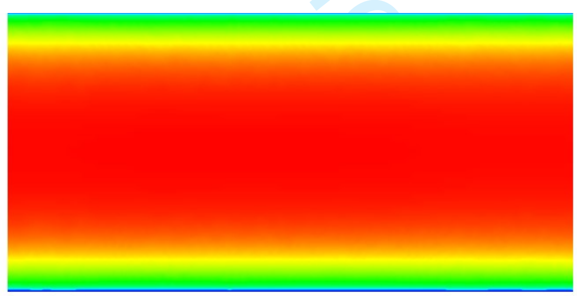

(h) P29%, channel width equal to 120 μm.

Figure 12: Internal potential (a-d) and horizontal velocity (e-h) distributions.

observed with smaller particles, whereas at 120 μm the difference between the two cases is reduced. At this channel width the maximum velocity is higher in the case of larger particles. This divergence can be attributed to the difference in permeability, that can be appreciated in Figure 10 by considering a particles diameter equal to 14 and 35 μm.

3.2.3 Effect of zeta potential on EOF

The zeta potential characterizing channel walls and solid particles significantly affects the internal potential distribution and, as a consequence, EOF. It should be noticed that in case of channels packed with porous media, a modified zeta potential is applied as a boundary condition to the channel walls. Its values, when channel walls and solid particles have the same zeta potential, are reported in Table 4.

Table 4: Modified zeta potential, ζ_w', calculated for different values of zeta potential acting on channel walls, ζ_w, and solid particles, ζ_p.

$\zeta_w = \zeta_p$ mV	ζ_w' mV
-5.00	-3.61
-10.00	-7.23
-19.00	-13.73
-30.00	-21.69
-50.00	-36.14
-75.00	-54.22

In Figure 13, the velocity profile is shown for free channels at several values of the walls zeta potential, and for channels packed with porous media at several values of walls and particles zeta potential.

The influence of the zeta potential on EO velocity is very low in the free channel and essentially null in channels packed with porous media. A different outcome is obtained when the zeta potential of walls, ζ_w and that of the particles ζ_p, are assumed to be different from each other. The modified zeta potential imposed on channel walls depend on both ζ_w and ζ_p. Its values for the two cases analysed are reported in Tables 5 (a) and (b).

First, a constant value of ζ_w is considered, whereas ζ_p is varied, as shown in Figure 14a. In this case, as ζ_p increases in absolute value, velocity increases. By keeping constant ζ_p and varying ζ_w, as illustrated in Figure 14b, EOF reduces as the difference between ζ_p and ζ_w increases, and, as expected, the velocity near the walls grows when ζ_w is much higher than ζ_p. This trend agrees with the results observed by Liapis and Grimes (2000), discussed in Section 1.

It is worth noticing that EO average velocity tends to decrease and to become constant as the zeta potential of solid particles increases and that of channel walls decreases. The velocity drops faster in case of variable

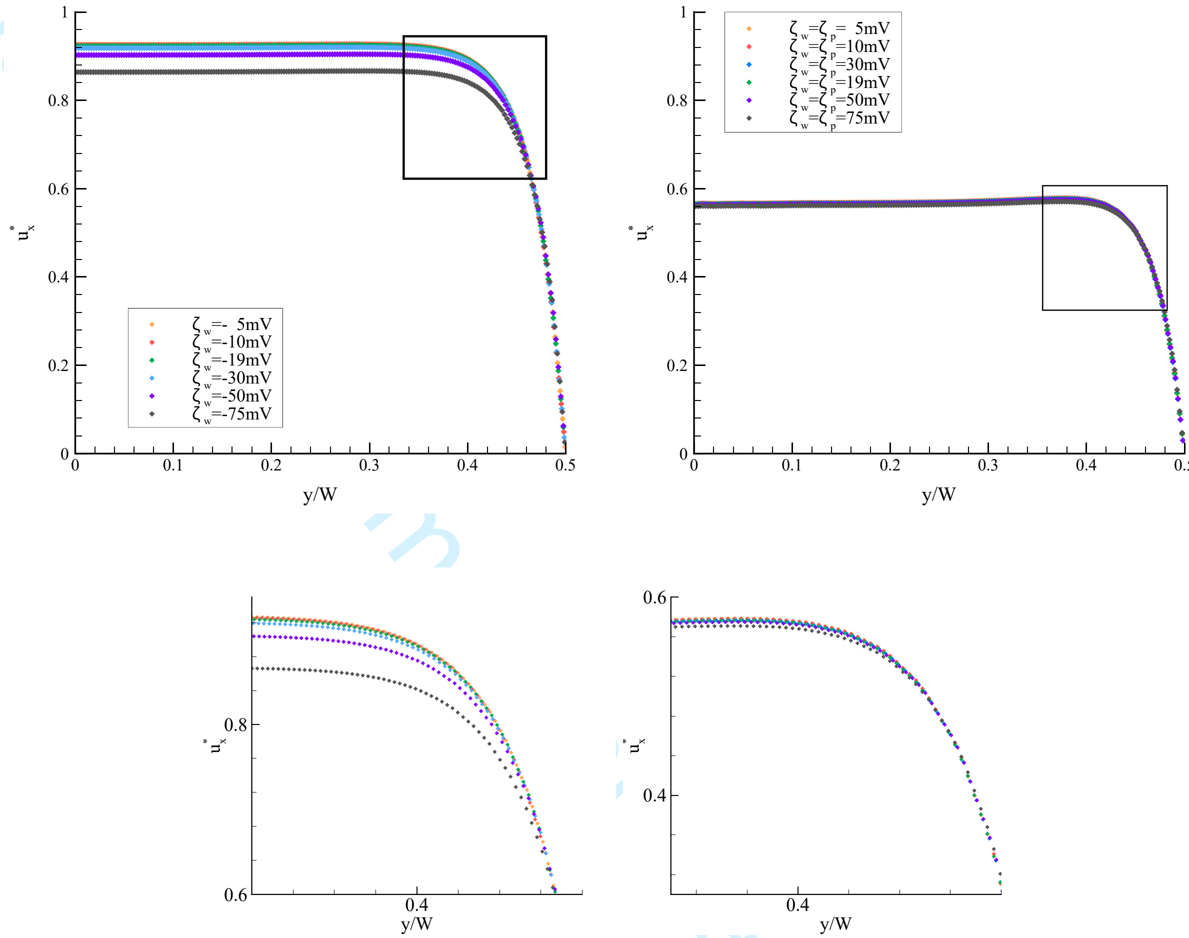

(a) Free channel. (b) Porous media channel.

Figure 13: EO velocity at different values of zeta potential, considering the same quantity for channel walls and solid particles.

Table 5: Modified zeta potential, ζ'_w, calculated for different values of zeta potential acting on channel walls, ζ_w, and solid particles, ζ_p.

(a) ζ_w = -19mV

ζ_p mV	ζ'_w mV
-5	-17.61
-10	-16.23
-19	-13.73
-30	-10.69
-50	-5.14
-75	1.78

(b) ζ_p = -19mV

ζ_w mV	ζ'_w mV
-5	0.6
-10	-4.23
-19	-13.73
-30	-24.73
-50	-44.73
-75	-69.73

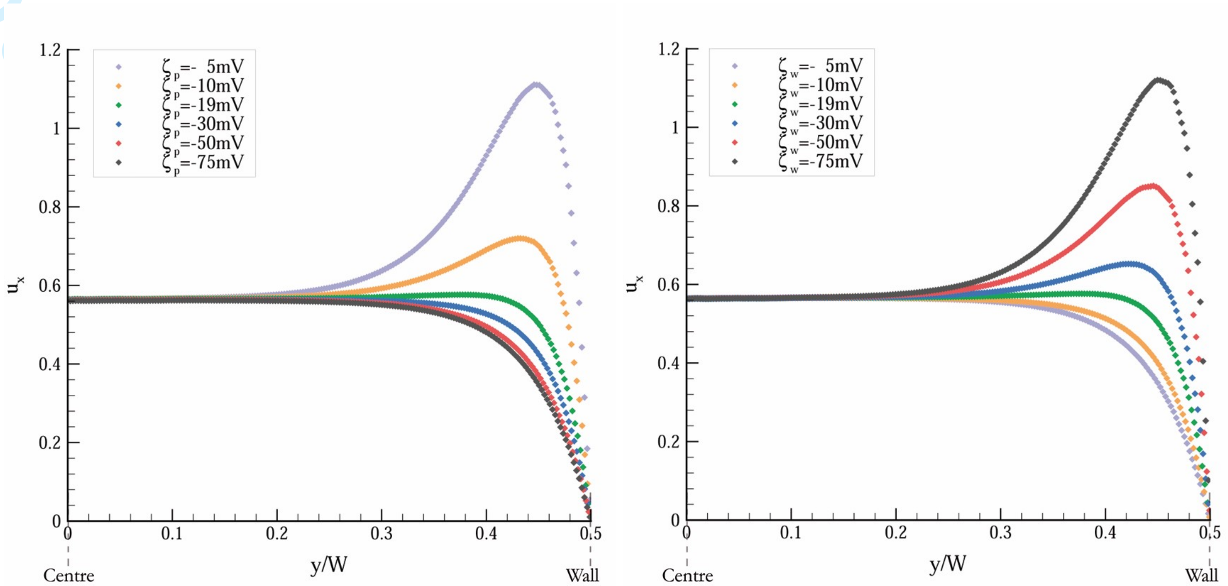

(a) Fixed ζ_w, variable ζ_p. (b) Fixed ζ_p, variable ζ_w.

Figure 14: Velocity at different values of zeta potential of solid particles and channel walls.

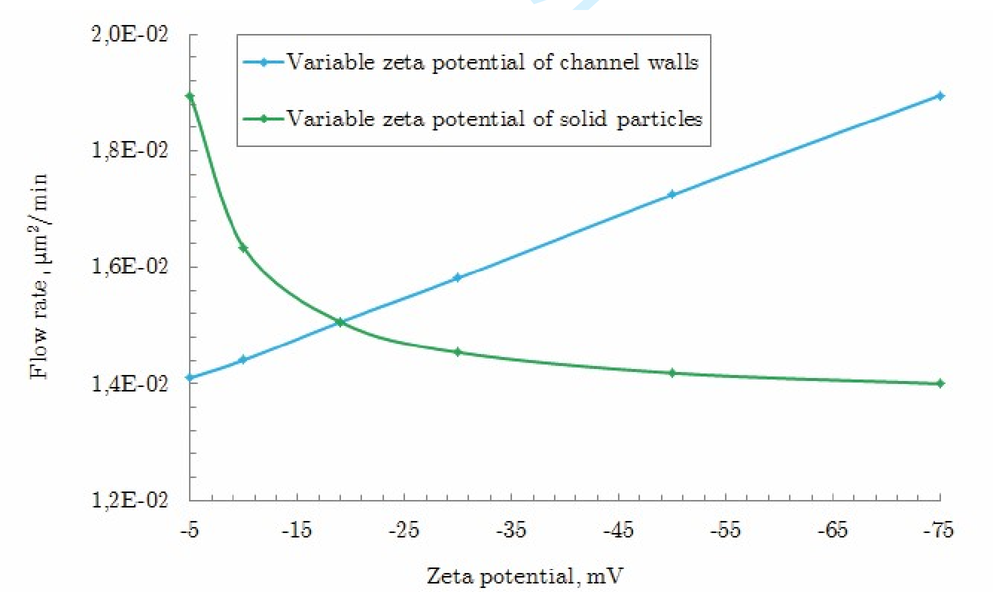

Figure 15: Flow rate at different values of modified zeta potential, with varying zeta potential of channel walls and solid particles.

ζ_w, as confirmed by the plot in Figure 15. Flow rate rapidly decreases as ζ_p increases in absolute value up to -30 mV, then it becomes approximately constant. For fixed ζ_p, the flow rate linearly increases with ζ_w.

3.2.4 Effect of bulk ionic concentration on EOF

The bulk ionic concentration influences the thickness of EDL or Debye length, κ^{-1}. As seen before, this parameter strongly affects EOF. For this reason, in many studies the dependence between the electro-kinetic radius, κW, and EOF has been analysed. Its effect on the velocity is assessed in free channels and channels packed with porous media.

In the analysis of EOF through porous media also the parameter κR_{pore} is taken into account, where R_{pore} is the hydraulic radius, defined in Eq. (16). This quantity affects the modified zeta potential, ζ_w', imposed on the channels walls.

The variation of both κW and κR_{pore}, and of ζ_w' , with bulk ionic concentration is reported in Table 6.

Table 6: Values of electro-kinetic radius, electro-kinetic hydraulic radius, and modified zeta potential, for different bulk ionic concentrations.

Bulk ionic concentration n_0 M	Electro-kinetic radius κW -	Electro-kinetic hydraulic radius κR_{pore} -	Modified zeta potential ζ_w' mV
$0.5E-05$	7.06	1.51	-3.89
$1.0E-05$	9.98	2.13	-6.20
$0.5E-04$	22.3	4.76	-12.0
$1.0E-04$	31.6	6.73	-13.9
$0.5E-03$	70.6	15.1	-16.8
$1.0E-03$	99.8	21.3	-17.5

The effect of bulk ionic concentration on horizontal velocity in free channels and channels packed with porous media is shown in Figure 16.

In free channels the average velocity initially increases at increasing bulk ionic concentration, then it starts to decrease. On the contrary, in channels packed with porous media the average velocity increases for increasing bulk ionic concentration in the whole range analysed. As mentioned above, the bulk ionic concentration affects the modified zeta potential, considered in channels packed with porous media. The influence of the zeta potential applied on the channel walls is highlighted in Figure 17, where both the modified zeta potential and the flow rate are plotted against the bulk concentration.

The effect of bulk ionic concentration on EOF can be better understood by analysing the internal potential results illustrated in Figure 18.

At lower concentrations, the EDL thickness is larger and the internal potential is not equal to zero in a larger fraction of the channel, as shown in Figure 18a. Despite this, the maximum absolute value of internal po-

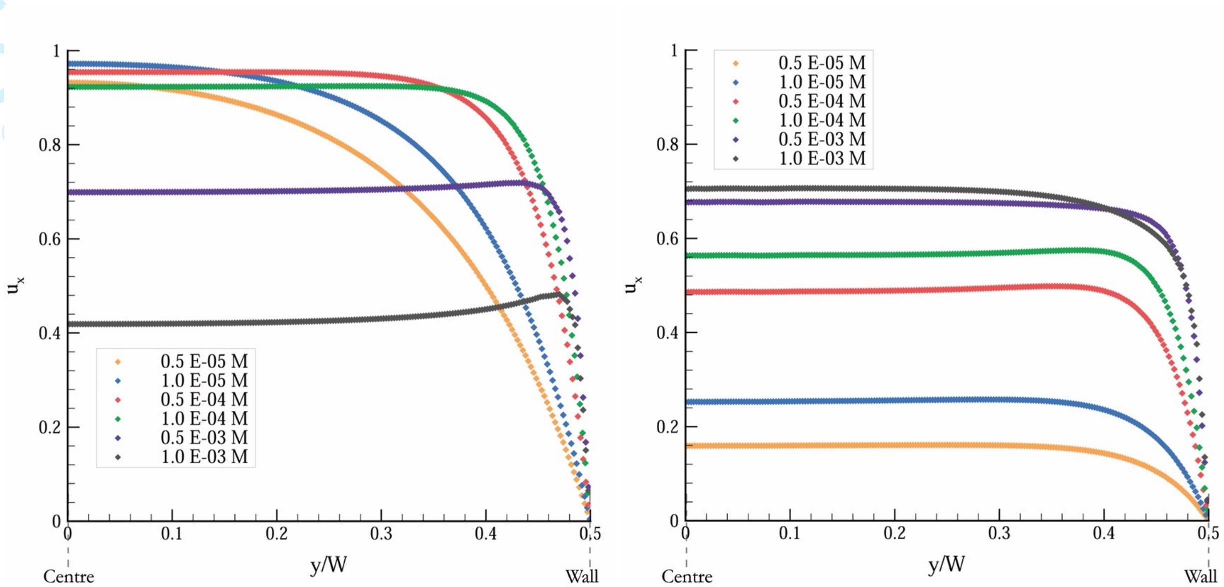

(a) Free channel. (b) Porous media channel.

Figure 16: EO velocity at different values of bulk ionic concentration.

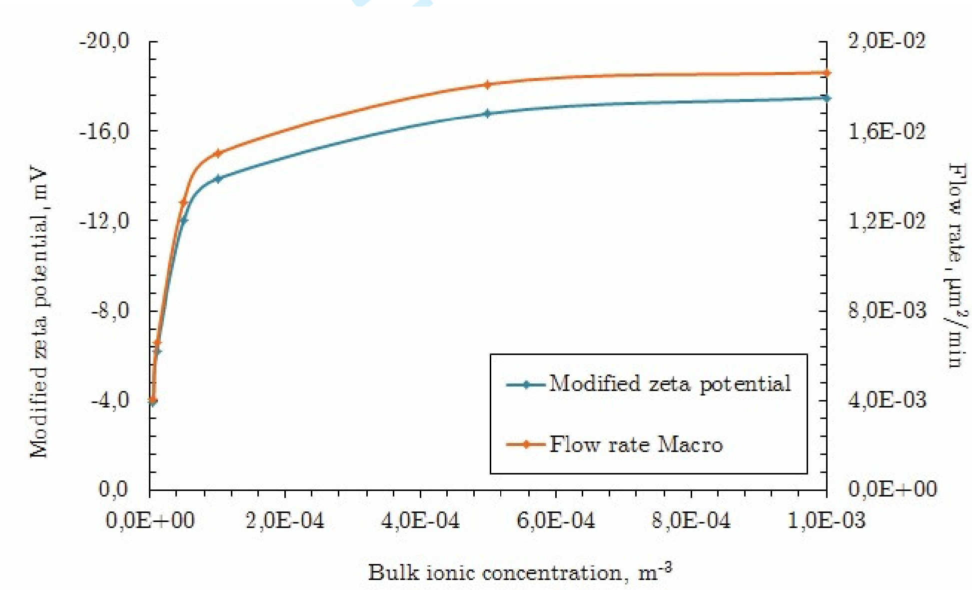

Figure 17: Modified zeta potential and flow rate at different values of bulk ionic concentration.

tential, equivalent to the modified zeta potential applied, is lower than that observed at higher concentration (Figure 18b), and, as a consequence, the average velocity within the channel is lower.

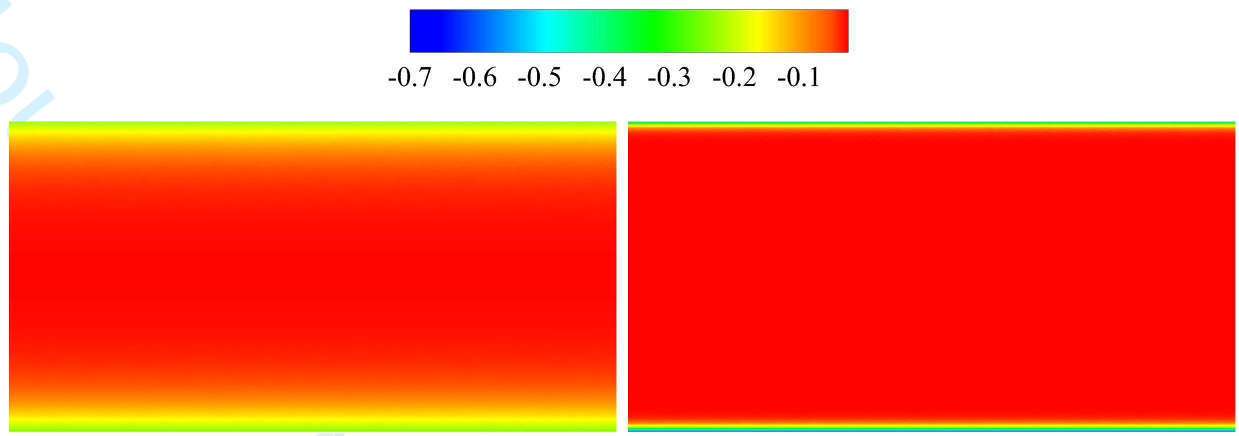

(a) n_0 = 1.0 E-05 M. (b) n_0 = 0.5 E-03 M.

Figure 18: Internal potential in channels packed with porous media at different values of bulk ionic concentration.

4 Conclusions

In this work electro-osmotic flow through porous media is analysed. The porous medium is assumed as a continuum and fluid flow is modelled through the generalized model for porous media flows, modified to take into account the electro-kinetic effects.

The developed model is used to evaluate the effectiveness of using electro-osmosis to drive flow through porous media. The results show that beyond a channel width of $100\mu m$, the charge of particles composing the porous medium is the main responsible for electro-osmotic flow. This means that electro-osmosis through porous media can be employed independently of the scale of the system, contrary to what occurs in free channels, where electro-osmotic flow decreases as the size of the channel increases. The influence of other parameters is also assessed. The particle size, which affects both the electro-kinetic effect and the flow, is varied to understand its effect on electro-osmotic flow. The electric fluid-solid interaction is taken into account through the zeta potential imposed on the channel walls, used to derive the internal potential distribution. In smaller micro-channels, particle size significantly affects electro-osmotic flow, while at larger channel widths the average velocity appears to be independent of the particle size.

The electric fluid-solid interaction is analysed also by directly considering the variation of zeta potential of both channel walls and solid particles. When these two quantities are identical, the fluid flow does not vary, while if they assume different values, flow can be enhanced. As the difference between the zeta potential of channel walls and that of solid particles increases, the maximum velocity grows. The flow rate increases at higher absolute values of zeta potentials on the channel walls, while it decreases and reaches a constant value when the absolute value of zeta potential of solid particle increases.

Finally, the influence of bulk ionic concentration of the solution on electro-kinetic effect and fluid flow is studied. As this quantity increases, the average velocity presents a rapid initial increase and then becomes approximately constant.

The results obtained from the numerical simulation of electro-osmotic flow in porous media can be used to

Roman symbol	Unit	Description
$b,\ d$	-	Numerical constants
c	$m \cdot s^{-1}$	Speed of sound
c_F	-	Forchheimer coefficient
c_m	$Moles$	Molar concentration
d_p	m	Particle size
Da		Darcy number
e	C	Elementary charge
E_x	$V \cdot m^{-1}$	External electric field
I		Bessel function
J		Non dimensional parameter
K	$m \cdot s^{-2}$	Permeability
k_{Bo}	$m^2 kg \cdot (s^2 K)^{-1}$	Boltzmann's constant
L	m	Length
n^+		Positive ions
n^-		Negative ions
n_0	m^{-3}	Ionic number concentration
N_A		Avogadro constant
p	$N \cdot m^{-2}$	Pressure
P		Porous term
R_{pore}	m	Average pore size
Re		Reynolds number
T	K	Temperature
u	$m \cdot s^{-1}$	Velocity
$\mathbf{V}$	$m \cdot s^{-1}$	Velocity vector
W	m	Channel width
z	-	Valence of the ions
Z	-	Non-dimensional parameter

define the best geometric and operating conditions for flow enhancement, demonstrating that the proposed generalised model can be useful as a tool for the optimization of electro-osmotic flow driven systems.

References

Al-Fariss, T. and Pinder, K. (1987). Flow through porous media of a shear-thinning liquid with yield stress. *The Canadian Journal of Chemical Engineering*, 65(3):391–405.

Anderson, J. L. and Keith Idol, W. (1985). Electroosmosis through pores with nonuniformly charged walls. *Chemical Engineering Communications*, 38(3-6):93–106.

Arnold, A. K. (2007). *Numerical Modelling of Electro-osmotic Flow through Micro-channels*. PhD Thesis, School of Engineering, Swansea University, UK.

Bennacer, R., Carcadea, E., Ene, H., Ingham, D., Lazar, R., Ma, L., Pourkashanian, M., and Stefanescu, I. (2007). A computational fluid dynamics analysis of a pem fuel cell system for power generation. *International Journal of Numerical Methods for Heat & Fluid Flow*, 17(3):302–312.

Acronyms	Description
AC	Alternating Current
CBS	Characteristic Based Split
CEC	Capillary ElectroChromatography
EDL	Electrical Double Layer
EO	Electro-Osmosis
EOF	Electro-Osmotic Flow
LBM	Lattice Boltzmann Method
REV	Representative Elementary Volume

Greek symbol	Unit	Description
β	-	Artificial compressibility parameter
ε	-	Dielectric constant
ε_0	$C \cdot (V \cdot m)^{-1}$	Permittivity of the vacuum
ζ	V	Zeta potential
ζ'	V	Modified Zeta potential
η	-	Numerical constant
κ		Debye length
λ	m	Brinkmann screening length
μ	$Pa \cdot s$	Viscosity
ϕ	V	External electric potential
Φ	-	Porosity
ρ_f	$kg \cdot m^{-3}$	Fluid density
ρ_e	$C \cdot m^{-3}$	Net charge density
$\rho_e ff$	$C \cdot m^{-3}$	Effective charge density
σ	$S \cdot m^{-1}$	Electrical Conductivity
τ	-	Tortuosity
ψ	V	EDL potential

Subscript symbol	Description
B	Brinkmann
chan	Channel
conv	Convective
cp	Charged particles
cw	Charged walls
d	Darcy
diff	Diffusive
e	Net
eff	Effective
f	Fluid
ref	Reference
p	Particle
w	Walls

Berrouche, Y., Avenas, Y., Schaeffer, C., Chang, H.-C., and Wang, P. (2009). Design of a porous electroosmotic pump used in power electronic cooling. *Industry Applications, IEEE Transactions on*, 45(6):2073–2079.

Brinkman, H. (1949). A calculation of the viscous force exerted by a flowing fluid on a dense swarm of particles. *Applied Scientific Research*, 1(1):27–34.

Cameselle, C. (2015). Enhancement of electro-osmotic flow during the electrokinetic treatment of a contaminated soil. *Electrochimica Acta*, 181:31–38.

Chai, Z., Guo, Z., and Shi, B. (2007). Study of electro-osmotic flows in microchannels packed with variable porosity media via Lattice Boltzmann method. *Journal of applied physics*, 101(10):104913.

Cheema, T., Kim, K., Kwak, M., Lee, C., Kim, G., and Park, C. (2013). Numerical investigation on electroosmotic flow in a porous channel. In *The 1st IEEE/IIAE International Conference on Intelligent Systems and Image Processing 2013 (ICISIP2013)*.

Chen, S., He, X., Bertola, V., and Wang, M. (2014). Electro-osmosis of non-newtonian fluids in porous media using Lattice Poisson–Boltzmann method. *Journal of colloid and interface science*, 436:186–193.

Darcy, H. (1856). *Les fontaines publiques de la ville de Dijon: exposition et application...* Victor Dalmont.

Di Fraia, S., Massarotti, N., and Nithiarasu, P. (2017). Effectiveness of flow obstructions in enhancing electro-osmotic flow. *Microfluidics and Nanofluidics*, 21(3).

Di Fraia, S., Massarotti, N., and Nithiarasu, P. (2018). Modelling electro-osmotic flow in porous media: A review. *International Journal of Numerical Methods for Heat and Fluid Flow*, 28(2):472–497.

Ehlers, W. and Bluhm, J. (2013). *Porous media: theory, experiments and numerical applications*. Springer Science & Business Media.

Eng, P. and Nithiarasu, P. (2009). Numerical investigation of an electroosmotic flow (EOF)–based micro-cooling system. *Numerical Heat Transfer, Part B: Fundamentals*, 56(4):275–292.

Ergun, S. and Orning, A. A. (1949). Fluid flow through randomly packed columns and fluidized beds. *Industrial & Engineering Chemistry*, 41(6):1179–1184.

Forchheimer, P. (1901). Wasserbewegung durch boden. *Z. Ver. Deutsch. Ing*, 45(1782):1788.

Grimes, B., Meyers, J., and Liapis, A. (2000). Determination of the intraparticle electroosmotic volumetric flow-rate, velocity and peclet number in capillary electrochromatography from pore network theory. *Journal of Chromatography A*, 890(1):61–72.

Herschel, W. H. and Bulkley, R. (1926). Consistency measurements of rubber-benzol solutions. *Colloid & Polymer Science*, 39(4):291–300.

Hlushkou, D., Apanasovich, V., Seidel-Morgenstern, A., and Tallarek, U. (2006). Numerical simulation of electrokinetic microfluidics in colloidal systems. *Chemical Engineering Communications*, 193(7):826–839.

Hlushkou, D., Seidel-Morgenstern, A., and Tallarek, U. (2005). Numerical analysis of electroosmotic flow in dense regular and random arrays of impermeable, nonconducting spheres. *Langmuir*, 21(13):6097–6112.

Hsu, C. and Cheng, P. (1990). Thermal dispersion in a porous medium. *International Journal of Heat and Mass Transfer*, 33(8):1587–1597.

Kang, Y., Tan, S. C., Yang, C., and Huang, X. (2007). Electrokinetic pumping using packed microcapillary. *Sensors and Actuators A: Physical*, 133(2):375–382.

Kang, Y., Yang, C., and Huang, X. (2004a). AC electroosmosis in microchannels packed with a porous medium. *Journal of Micromechanics and Microengineering*, 14(8):1249.

Kang, Y., Yang, C., and Huang, X. (2004b). Analysis of the electroosmotic flow in a microchannel packed with homogeneous microspheres under electrokinetic wall effect. *International journal of engineering science*, 42(19):2011–2027.

Kang, Y., Yang, C., and Huang, X. (2005). Analysis of electroosmotic flow in a microchannel packed with microspheres. *Microfluidics and Nanofluidics*, 1(2):168–176.

Kozak, M. W. and Davis, E. J. (1986). Electrokinetic phenomena in fibrous porous media. *Journal of colloid and interface science*, 112(2):403–411.

Kozak, M. W. and Davis, E. J. (1989). Electrokinetics of concentrated suspensions and porous media: I. thin electrical double layers. *Journal of colloid and interface science*, 127(2):497–510.

Lewis, R. and Garner, R. (1972). A finite element solution of coupled electrokinetic and hydrodynamic flow in porous media. *International Journal for Numerical Methods in Engineering*, 5(1):41–55.

Lewis, R. W. and Humpheson, C. (1973). Numerical analysis of electro-osmotic flow in soils. *Journal of Soil Mechanics & Foundations Div*, 99(Proc Paper).

Li, B., Zhou, W., Yan, Y., Han, Z., and Ren, L. (2013a). Numerical modelling of electroosmotic driven flow in nanoporous media by Lattice Boltzmann method. *Journal of Bionic Engineering*, 10(1):90–99.

Li, B., Zhou, W., Yan, Y., and Tian, C. (2013b). Evaluation of electro-osmotic pumping effect on microporous media flow. *Applied Thermal Engineering*, 60(1):449–455.

Li, D. and Remcho, V. T. (1997). Perfusive electroosmotic transport in packed capillary electrochromatography: Mechanism and utility. *Journal of Microcolumn Separations*, 9(5):389–397.

Liapis, A. I. and Grimes, B. A. (2000). Modeling the velocity field of the electroosmotic flow in charged capillaries and in capillary columns packed with charged particles: interstitial and intraparticle velocities in capillary electrochromatography systems. *Journal of Chromatography A*, 877(1):181–215.

541 Liu, S. and Masliyah, J. H. (1996). Single fluid flow in porous media. *Chemical Engineering Communications*, 148(1):653–732.

543 Mahmud Hasan, A., Wahab, M., and Guo, S. (2011). CFD analysis of a PEM fuel cell for liquid dispersion at the interface of GDL-GFC. *International Journal of Numerical Methods for Heat & Fluid Flow*, 21(7):810–821.

546 Massarotti, N., Arpino, F., Lewis, R. W., and Nithiarasu, P. (2006). Explicit and semi-implicit CBS procedures for incompressible viscous flows. 66(10):1618–1640.

548 Massarotti, N., Nithiarasu, P., and Carotenuto, A. (2003). Microscopic and macroscopic approach for natural convection in enclosures filled with fluid saturated porous medium. *International Journal of Numerical Methods for Heat & Fluid Flow*, 13(7):862–886.

551 Misra, J. and Chandra, S. (2013). Electro-osmotic flow of a second-grade fluid in a porous microchannel subject to an ac electric field. *Journal of Hydrodynamics, Ser. B*, 25(2):309–316.

553 Nield, D. A. and Bejan, A. (2006). *Convection in porous media*. Springer Science & Business Media.

554 Nithiarasu, P. (2003). An efficient artificial compressibility (AC) scheme based on the characteristic based split (CBS) method for incompressible flows. 56(13):1815–1845.

556 Nithiarasu, P., Lewis, R. W., and Seetharamu, K. N. (2016). *Fundamentals of the Finite Element Method for Heat and Mass Transfer*. Wiley, second edition.

558 Nithiarasu, P., Seetharamu, K., and Sundararajan, T. (1996). Double-diffusive natural convection in an enclosure filled with fluid-saturated porous medium: A generalized Non-Darcy approach. *Numerical Heat Transfer, Part A - Applications*, 30:413–426.

561 Nithiarasu, P., Seetharamu, K., and Sundararajan, T. (1997). Natural convective heat transfer in a fluid saturated variable porosity medium. *International Journal of Heat and Mass Transfer*, 40(16):3955–3967.

564 Patankar, N. A. and Hu, H. H. (1998). Numerical simulation of electroosmotic flow. *Analytical Chemistry*, 70(9):1870–1881.

566 Probstein, R. F. (2005). *Physicochemical hydrodynamics: an introduction*. John Wiley & Sons.

567 Qu, W. and Li, D. (2000). A model for overlapped EDL fields. *Journal of Colloid and Interface Science*, 224(2):397–407.

569 Rathore, A. and Horváth, C. (1997). Capillary electrochromatography: theories on electroosmotic flow in porous media. *Journal of Chromatography A*, 781(1):185–195.

571 Rice, C. and Whitehead, R. (1965). Electrokinetic flow in a narrow cylindrical capillary. *The Journal of Physical Chemistry*, 69(11):4017–4024.

Scales, N. and Tait, R. N. (2006). Modeling electroosmotic and pressure-driven flows in porous microfluidic devices: Zeta potential and porosity changes near the channel walls. *The Journal of chemical physics*, 125(9):094714.

Shapiro, A. P. and Probstein, R. F. (1993). Removal of contaminants from saturated clay by electroosmosis. *Environmental Science & Technology*, 27(2):283–291.

Tallarek, U., Rapp, E., Seidel-Morgenstern, A., and Van As, H. (2002). Electroosmotic flow phenomena in packed capillaries: from the interstitial velocities to intraparticle and boundary layer mass transfer. *The Journal of Physical Chemistry B*, 106(49):12709–12721.

Tang, G., Ye, P., and Tao, W. (2010). Pressure-driven and electroosmotic non-Newtonian flows through microporous media via Lattice Boltzmann method. *Journal of Non-Newtonian Fluid Mechanics*, 165(21):1536–1542.

Vafai, K. (2005). *Handbook of Porous Media*. CRC Press.

Vafai, K. and Tien, C. (1981). Boundary and inertia effects on flow and heat transfer in porous media. *International Journal of Heat Mass Transfer*, 24:195–203.

Wan, Q.-H. (1997). Capillary electrochromatography: effect of electrolyte concentration on electroosmotic flow and column efficiency. *Journal of Chromatography A*, 782(2):181–189.

Wang, P., Chen, Z., and Chang, H.-C. (2006). A new electro-osmotic pump based on silica monoliths. *Sensors and Actuators B: Chemical*, 113(1):500–509.

Whitaker, S. (1967). Diffusion and dispersion in porous media. *AIChE Journal*, 13(3):420–427.

Wu, R. C. and Papadopoulos, K. D. (2000). Electroosmotic flow through porous media: Cylindrical and annular models. *Colloids and Surfaces A: Physicochemical and Engineering Aspects*, 161(3):469–476.

Yang, C. and Li, D. (1998). Analysis of electrokinetic effects on the liquid flow in rectangular microchannels. *Colloids and surfaces A: physicochemical and engineering aspects*, 143(2):339–353.

Yang, R.-J., Fu, L.-M., and Lin, Y.-C. (2001). Electroosmotic flow in microchannels. *Journal of colloid and interface science*, 239(1):98–105.

Yao, S., Myers, A. M., Posner, J. D., Rose, K. A., and Santiago, J. G. (2006). Electroosmotic pumps fabricated from porous silicon membranes. *Microelectromechanical Systems, Journal of*, 15(3):717–728.

Yao, S. and Santiago, J. G. (2003). Porous glass electroosmotic pumps: theory. *Journal of Colloid and Interface Science*, 268(1):133–142.

Zeng, S., Chen, C.-H., Mikkelsen, J. C., and Santiago, J. G. (2001). Fabrication and characterization of electroosmotic micropumps. *Sensors and Actuators B: Chemical*, 79(2):107–114.